

Abstract

We investigate how spatial variations in tidal heating affect Io's isostatic topography at long wavelengths. The difference between the hydrostatic shape implied by Io's gravity field and its observed global shape is less than the latter's 0.3 km uncertainty. Assuming Airy isostasy, degree-2 topography < 300 m amplitude is only possible if surface heat flux varies spatially by < 17% of the mean value. This is consistent with Io's volcano distribution and is possible if tidal heat is generated within a convecting layer underneath the lithosphere. However, that layer would require a viscosity < 10^{10} Pa s. A magma ocean would have low enough viscosity but would not generate enough tidal heat internally. Conversely, assuming Pratt isostasy, we find ~150 m degree-2 topography is easily achievable. If a magma ocean was present, Airy isostasy would dominate; we therefore conclude that Io is unlikely to possess a magma ocean.

Plain Language Summary

As it orbits Jupiter elliptically, the difference in gravitational pull experienced by the moon Io results in tidal heating due to internal friction. Some evidence suggests this heat forms a magma ocean beneath Io's crust. If so, there would be a difference in the amount of heat generated at Io's equator versus its poles and would alter the thickness of Io's crust between the two locales. Assuming the crust has a uniform density, its thickness would be inversely proportional to the tidal heat beneath the crust, which in turn affects the difference in Io's radius at the equator versus at its poles. However, reasonable variation in tidal heating across Io would result in a greater difference in radius than is observed. The difference in observed radius is more likely if variation in tidal heat across Io affects crustal density rather than crustal thickness. Then, it is more likely that Io does not have a magma ocean.

1 Introduction

It is presently a mystery whether Jupiter's hyper-volcanic satellite, Io, hides a magma ocean beneath its lithosphere (e.g., de Kleer et al., 2019; Matusyama et al., 2022). Potential evidence for such a magma ocean includes a magnetic induction signal measured by the Galileo spacecraft mission; however, such a signal could also be indicative of a magmatic sponge layer that is a mix of rock and melt (Khurana et al., 2011). Moreover, the distribution of volcanoes on Io's surface may be indicative of a concentration of tidal dissipation in

43 the shallow mantle (e.g., Tackley et al., 2001; Tyler et al., 2015). Miyazaki and Stevenson
44 (2022) argue such a distribution could instead be the result of heterogeneities in lithospheric
45 weakness, as the presence of a magma ocean may redistribute any spatial variations in
46 tidal heating due to said magma ocean. Further, they argue that a partial-melt layer within
47 Io’s subsurface is inherently unstable and would instead separate into a solid and liquid
48 phase (Miyazaki & Stevenson, 2022). The presence of a magma ocean within Io’s subsurface
49 would have implications for the distribution and transport of tidal heating within the
50 satellite (e.g., Matusyama et al., 2022).

51 In recent work, Gyalay and Nimmo (2023) demonstrated how to use the observed
52 long-wavelength topography of Saturn’s icy satellites to infer the tidal heating distribution
53 beneath their ice shells, which provides an indirect window into their interior structure.
54 We first investigate if such a methodology may be applied to Io by assuming Io’s degree-2
55 shape is a combination of its hydrostatic shape (due to Io’s rotational flattening and tidal
56 buldge) and topographic variations due to the spatial pattern of tidal heating. Upon subtraction
57 of Io’s hydrostatic shape, however, we find the remnant topography is lower than the uncertainty
58 in Io’s global shape (see Section S2 of Supplement 1). While we thus cannot meaningfully
59 apply the methodology of Gyalay and Nimmo (2023a), the uncertainty nonetheless places
60 a useful upper bound on the amplitude of topography that spatial variations tidal heating
61 may produce. We use this constraint to make a prediction on the presence or absence
62 of a magma ocean that may be confirmed by upcoming Juno flybys (Keane et al., 2022).
63 In particular, we find that Airy isostasy produces topographic amplitudes that are too
64 large, while Pratt isostasy does not. Since Airy isostasy is likely to dominate if a magma
65 ocean is present, we conclude that Io probably lacks a magma ocean.

66 **2 Background**

67 The spatial variation of tidal heating across a satellite depends greatly on the depth
68 or thickness of the tidal-heat-producing region (e.g., the crust, lithosphere, aesthenosphere,
69 etc.), whether the tidal-heat-producing region overlies a more rigid (e.g., rocky mantle)
70 or a more fluid (e.g., magma ocean) layer, and whether the tides are caused by the satellite’s
71 eccentricity (orbit’s ellipticity) or obliquity (tilt of the satellite’s spin axis relative to the
72 normal of its orbital plane) (e.g., Segatz et al., 1988; Beuthe, 2013). In recent work, Gyalay
73 and Nimmo (2023a) demonstrated the use of the observed long-wavelength topography
74 of Saturn’s icy satellites to infer the tidal heating distribution beneath their ice shells.

75 In principle, a similar methodology could be applied to Io’s topography in order to test
 76 whether it was the result of spatial variations in tidal heating consistent with a magma
 77 ocean beneath Io’s lithosphere.

78 Previous studies have investigated the link between Io’s tidal heating and its lithospheric
 79 thickness (Steinke et al., 2020a; Spencer et al., 2021), where the lithospheric thickness
 80 can be related to topography under the assumption of isostasy (see the next section, Section
 81 3). The average surface heat flow of Io is at least 2 W m^{-2} (Veeder et al., 1994; Simonelli
 82 et al., 2001; McEwen et al., 2004; Rathbun et al., 2004; de Kleer et al., 2019). This significant
 83 quantity of heat is generated frictionally by tidal stresses as a result of Io’s Laplace resonance
 84 with Europa and Ganymede (predicted by Peale et al., 1979, mere weeks before Voyager
 85 1’s flyby). This tidal heating vastly dominates the surface heat flow, which would be only
 86 0.016 W m^{-2} if Io’s entire mass had the radioactive heat production rate of Earth’s mantle
 87 (7.38 pW kg^{-1} , e.g., Turcotte & Schubert, 2014). As Io’s core is not radioactive, even
 88 that value is an upper bound.

89 If tidal heat were simply conducted to the surface, the lithosphere would need to
 90 be less than a few km thick (e.g., O’Reilly & Davies, 1981). However, Io’s surface is dotted
 91 with mountains that can reach heights $> 10 \text{ km}$ (e.g., Carr et al., 1979, 1998; Schenk
 92 et al., 2001). In Section S1 of Supplement 1, we estimate that this requires a minimum
 93 lithosphere thickness of 23 km (cf. values of $14\text{-}50 \text{ km}$ in Nash et al., 1986; Keszthelyi
 94 & McEwen, 1997; Carr et al., 1998; Jaeger et al., 2003; McEwen et al., 2004). O’Reilly
 95 and Davies (1981) argued that to satisfy the seemingly-paradoxical, observed constraints
 96 of Io’s mountainous terrain and high surface heat flux, Io must advect much of its heat
 97 through a thick, cold lithosphere via heat pipes of magma that erupt upon the surface.
 98 Spencer et al. (2021) incorporated this effect into their study by using melt production
 99 from tidal dissipation to heat the lithosphere and predict surface topography. Our approach
 100 differs from theirs in a few key ways, as elaborated upon below.

101 We make the simplifying assumption that if tidal heating operates at the base of
 102 the lithosphere or deeper, it provides a total surface heat flux F as described by Equations
 103 1 and 3b of O’Reilly and Davies (1981):

$$F = v\rho[\Delta H_f + C_p(T_m - T_s)] + \frac{v\rho C_p(T_m - T_s)}{e^{vd/\kappa} - 1}, \quad (1)$$

104 where v is the resurfacing rate, ρ is the magma density, ΔH_f is the latent heat of fusion,
 105 C_p is the specific heat, T_m is the melting temperature, T_s is the surface temperature, κ

Table 1. Variables and their (Preferred) Values

	Variable	(Pref.) Value	Note
F	Surface heat flux	$F_0 > 2 \text{ W m}^{-2}$	Observed ^a
d	Lithosphere thickness	$d_0 > 23 \text{ km}$	Section S1 of Supplement 1
v	Volcanic emplacement rate	$v_0 > 10.7 \text{ mm yr}^{-1}$ ($v_0 > 0.34 \text{ nm s}^{-1}$)	Eq. 1 for $d = 23 \text{ km}$, $F = 2 \text{ W m}^{-2}$
ρ	Magma density	$3,000 \text{ kg m}^{-3}$	O'Reilly and Davies (1981)
$\Delta\rho$	Density contrast	300 kg m^{-3}	
ΔH_f	Latent heat of fusion	450 kJ kg^{-1}	O'Reilly and Davies (1981)
C_p	Specific heat	$1 \text{ kJ kg}^{-1} \text{ K}^{-1}$	O'Reilly and Davies (1981)
T_s	Surface temperature	110 K	Rathbun et al. (2014)
T_m	Melting temperature	$T_m - T_s = 1,500 \text{ K}$	O'Reilly and Davies (1981)
k	Thermal conductivity	$3 \text{ W m}^{-1} \text{ K}^{-1}$	O'Reilly and Davies (1981)
κ	Thermal diffusivity	$10^{-6} \text{ m}^2 \text{ s}^{-1}$	O'Reilly and Davies (1981)
α	Volumetric thermal expansivity	$3 \times 10^{-5} \text{ K}^{-1}$	
Q_A	Activation energy	300 kJ mol^{-1}	
R_G	Universal gas constant	$8.3 \text{ J mol}^{-1} \text{ K}^{-1}$	
R_0	Io radius	$1,800 \text{ km}$	Observed
g	Surface gravity	1.8 m s^{-2}	Observed
C	Moment of Inertia	$0.3782 M R_0^2$	Schubert et al. (2004)

^aVeeder et al. (1994); Simonelli et al. (2001); McEwen et al. (2004); Rathbun et al. (2004);
de Kleer et al. (2019)

106 is the thermal diffusivity, and d the lithospheric thickness. One can also find the thermal
107 conductivity of the lithosphere k as $k = \rho C_p \kappa$. Table 1 lists our preferred values for these
108 variables, which borrow largely from O'Reilly and Davies (1981). The first term on the
109 right-hand side of Equation 1 provides the portion of heat flux that is advected through
110 heat pipes to the surface, while the second term provides the portion of heat flux that
111 is conducted through the lithosphere. In the limit of low volcanic emplacement v , we recover
112 Fourier's law of thermal conduction through a slab.

113 At a given lithospheric thickness, Equation 1 implies a larger volcanic emplacement
114 rate produces a higher heat flux; while for a given resurfacing/emplacement rate, the lithosphere

115 thins when tidal dissipation increases. The latter point can also be seen by inverting Equation
 116 1 to solve for d ,

$$d = \frac{\kappa}{v} \ln \left(\frac{v\rho C_p (T_m - T_s)}{F - v\rho [\Delta H_f + C_p (T_m - T_s)]} + 1 \right). \quad (2)$$

117 Equation 1 or 2 only satisfies both the minimum average surface heat flux $F > 2 \text{ W m}^{-2}$
 118 and our minimum average lithosphere thickness $d > 23 \text{ km}$ for Io when the conductive
 119 heat flux is a small fraction of the total heat flux, $F_{cond} < 3 \times 10^{-4} F$. Alternatively,
 120 one may simply state that the total heat flux is dominated by the advective term, $F \sim$
 121 F_{adv} . This requires an average volcanic emplacement rate of $v = 10.7 \text{ mm yr}^{-1}$ ($3.4 \times 10^{-10} \text{ m s}^{-1}$)
 122 when $F = 2 \text{ W m}^{-2}$.

123 By inferring the spatial distribution of tidal heating from topography, we may make
 124 inferences about the interior structure of Io. But first we must isolate the portion of Io's
 125 topography that arises from variations in tidal heating. Tidal heating varies spatially in
 126 even-orders of spherical harmonic degrees 2 and 4. We would thus wish to analyze Io's
 127 topography in those same spherical harmonics (e.g., Gyalay & Nimmo, 2023a). Unfortunately,
 128 we find in Section S2 of Supplement 1 that after accounting for the hydrostatic component
 129 of Io's shape (i.e., that which is due to Io's tidal bulge and rotational flattening), Io's
 130 remaining topography in those spherical harmonics is less than the uncertainty in global
 131 shape. Any conclusion on patterns of tidal heating inferred from this topography is then
 132 meaningless.

133 However, the *magnitude* of topographic variation may still yield some important
 134 constraints. In our case, the maximum (non-hydrostatic) topographic variation is limited
 135 by the uncertainty in degree-2 shape, which is on the order of 0.3 km (Section S2 of Supplement
 136 1). In, e.g., Beuthe (2013), the heat flux due to tidal heating can vary spatially in magnitude
 137 on the order of its average value. Io would not be as hot as it is without significant tidal
 138 heating (Peale et al., 1979). Then it stands to reason that most (if not all) of Io's heat
 139 flow is due to tidal heating. Given some variation in tidal heating, we can calculate the
 140 expected variation in Io's topography and compare it to our bounds on the possible variation
 141 in Io's topography.

142 **3 Predicting Isostatic variation in Io's topography**

143 We make the assumption that Io's crust is in isostatic equilibrium at long wavelengths
 144 (low spherical harmonic degree). In any form of isostasy, we expect that either the total

145 mass or pressure at some depth to be constant across a planetary body despite variations
 146 in the topography (see, e.g., Hemingway & Masuyama, 2017, for an argument in favor
 147 of equal-pressure isostasy). An alternate treatment of isostasy seeks to minimize the deviatoric
 148 stress within the crust (Beuthe, 2021). Minimum-stress isostasy can be approximated
 149 by equal-weight isostasy, which returns results between those of equal-mass and equal-pressure
 150 isostasy. In Gyalay and Nimmo (2023a), we used both equal-mass and equal-pressure
 151 isostasy as endmember cases in examining the ice shell of Tethys. Ultimately, interpretation
 152 of Tethys' interior was consistent across both treatments of isostasy. However, as we do
 153 not expect a significantly thick lithosphere on Io relative to its total radius, constant-pressure
 154 isostasy and constant-mass isostasy are nearly identical. Therefore in this paper, we default
 155 to the simpler calculations using equal-mass isostasy.

156 Beyond the choice of equal-mass, equal-pressure, equal-weight, or minimum-stress
 157 isostasy, there are still two overarching types of isostasy: Airy isostasy wherein topography
 158 is due to crustal thickness variations (more likely in the case of a magma ocean) or Pratt
 159 isostasy where topography is due to crustal density variations. In this manuscript, we
 160 apply these isostatic assumptions to the entire lithosphere (i.e., both the crust *and* the
 161 uppermost layer of the mantle) rather than just the crust. We assume that the bulk density
 162 of the crust plus uppermost mantle can differ from that of the mantle beneath, because
 163 of petrological differences arising during melt production and transport. The presence
 164 of heat pipes transporting melt from the mantle to the surface further necessitate another
 165 assumption: the dependence of volcanic emplacement rate v upon variations in heat flow
 166 F . We examine two endmember states: either v is a constant value $v = v_0$, or v varies
 167 in direct proportion to the local surface heat flux $v = v_0 F / F_0$, where F_0 is the average
 168 heat flow. In comparison, Spencer et al. (2021)'s treatment of Pratt isostasy in Io's lithosphere
 169 makes the distinction between the abundance of heat pipes and the flux of melt through
 170 each heat pipe. They hold either the pipe density uniform (but allow flow to vary in each)
 171 or the flow through any pipe constant (but allow variation in the concentration of heat
 172 pipes). However, this extra flexibility requires the assumption of additional constants
 173 to relate the values to v . We avoid having to make such assumptions with our approach.

174 In the limit of strong tidal heating, the amplitude of heat flux variations δF in spherical
 175 harmonic degree-2 (where $\delta F = F - F_0$) approaches the average total heat flux F_0 (e.g.
 176 Beuthe, 2013). Then, we may test which of our cases predict isostatic topography as a
 177 function of spatial variations in tidal heating that is consistent with a maximum amplitude

178 of ~ 0.3 km. We plot the expected topography as a function of heat flux variation for
 179 each mode of isostasy (Pratt or Airy) and dependence of emplacement rate on local heat
 180 flux ($v = v_0$ or $v \propto F$) in Figure 1.

181 3.1 Airy Isostasy

182 If there is a sub-surface magma ocean, we would expect Airy isostasy as with the
 183 floating shells of icy satellites. Here, we assume the topography is driven by variations
 184 in lithospheric thickness. To maintain a constant pressure at depth, lithospheric thinning
 185 would result in negative surface topography, and vice versa. We can relate topography
 186 h to a change in lithospheric thickness δd :

$$h = \frac{\delta d}{\left(1 + \frac{\rho}{\Delta\rho}\right)}, \quad (3)$$

187 where $\Delta\rho$ is the density contrast between the lithosphere and the underlying material.
 188 If the magma is sourced from the upper mantle and is denser than the lithosphere, a topographic
 189 high is the result of a thicker lithosphere. If instead the magma is sourced from the base
 190 of the crust and is less dense than the lithosphere (as a whole), then this equation implies
 191 a topographic high is the result of a thinner lithosphere. However, that latter scenario
 192 is inherently unstable and subject to overturn of the lithosphere. We therefore assume
 193 the lithosphere is 300 kg m^{-3} less dense than the magma.

194 3.1.1 Constant v case

195 If we assume the emplacement rate v is uniform across Io's surface in the case of
 196 Airy isostasy, we can begin with Equation 2 to calculate the expected topography h for
 197 some given variation in heat flux δF from the mean F_0 . After setting $v = v_0$, the difference
 198 in lithospheric thickness δd calculated by subtracting the mean d_0 from Equation 2 is,

$$\delta d = \frac{\kappa}{v_0} \ln \left(\frac{v_0 \rho C_p (T_m - T_s)}{F_0 + \delta F - v_0 \rho [\Delta H_f + C_p (T_m - T_s)]} + 1 \right) - d_0. \quad (4)$$

199 Note that $v_0 \rho [\Delta H_f + C_p (T_m - T_s)]$ is the advective heat flux, F_{adv} . Then,

$$\delta d = \frac{\kappa}{v_0} \ln \left(\frac{v_0 \rho C_p (T_m - T_s) \frac{1}{F_0}}{1 + \frac{\delta F}{F_0} - \frac{F_{adv}}{F_0}} + 1 \right) - d_0. \quad (5)$$

200 Then because the conductive heat flux $F_{cond} = v \rho C_p (T_m - T_s) / (e^{vd/\kappa} - 1)$, we may
 201 further rearrange the equation and substitute δd into Equation 3 to find,

$$h = \frac{1}{1 + \frac{\rho}{\Delta\rho}} \left[\frac{\kappa}{v_0} \ln \left(\frac{\frac{F_{cond,0}}{F_0} e^{v_0 d_0 / \kappa} + \frac{\delta F}{F_0}}{\frac{F_{cond,0}}{F_0} + \frac{\delta F}{F_0}} \right) - d_0 \right], \quad (6)$$

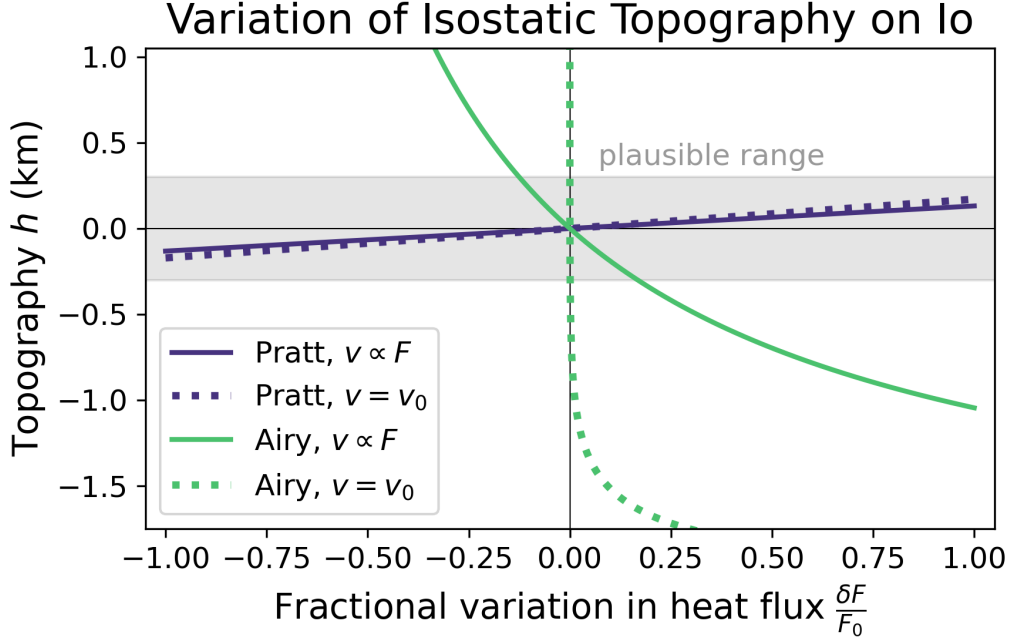


Figure 1. We plot the variation of Io’s isostatic long wavelength topography as a function of heat flux, as compared to the amplitude of topography $|h| < 0.3$ km allowed by the uncertainty in Io’s global shape (gray region). Topography that assumes Airy isostasy and $v = v_0$ (dotted green line) is characterized by Equation 6 for $F_{cond,0} = 2.95 \times 10^{-4} F_0$, which is the maximum value allowed for the minimum average lithospheric thickness $d_0 = 23$ km and minimum average heat flux $F_0 = 2 \text{ W m}^{-2}$. Increasing d_0 would further limit $F_{cond,0}$ and the maximum variability of δF . Topography that assumes Airy isostasy and $v \propto F$ (solid green line) is characterized by Equation 8 for minimum average lithospheric thickness $d_0 = 23$ km. Larger d_0 would increase topography as a function of heat flux variation. Topography that assumes Pratt isostasy and $v = v_0$ (dotted purple line) is characterized by Equation 21 for minimum average volcanic emplacement $v_0 = 10.7 \text{ mm yr}^{-1}$. Topography that assumes Pratt isostasy and $v \propto F$ is characterized by Equation 28 for the same assumed v_0 . Larger v_0 would reduce variation in h for both cases of Pratt isostasy. All other parameters use the preferred values in Table 1.

202 where $F_{cond,0}$ is F_{cond} at $d = d_0$ and $v = v_0$. Because F_{adv} remains constant if $v =$
 203 v_0 , then $|\delta F| < F_{cond,0}$, where $F_{cond,0} < 3 \times 10^{-4}$ for the preferred value of our parameters
 204 in Table 1. Further, in Equation 6 we can easily see that the topography is undefined
 205 if $\delta F = -F_{cond,0}$. Thus, it is impossible for tidal heat flux variations on the order of
 206 the average heat flux $|\delta F| \sim F_0$ to exist for an Io lithosphere under Airy isostasy with
 207 constant emplacement rate v_0 unless the total heat flux were dominated by the conductive
 208 term.

209 **3.1.2 $v \propto F$ case**

210 When v is instead proportional to F in the case of Airy isostasy, we substitute $v =$
 211 $v_0 F / F_0$ into Equation 1 and solve for F :

$$F = \frac{F_0 \kappa}{d v_0} \ln \left(\frac{v_0 \rho C_p (T_m - T_s)}{F_0 - v_0 \rho [\Delta H_f + C_p (T_m - T_s)]} + 1 \right). \quad (7)$$

212 When compared to Equation 2, we may simplify Equation 7 to $Fd = F_0 d_0$. Substituting
 213 $d = d_0 + \delta d$ and Equation 3 into Equation 7, we rearrange and find

$$h = \frac{-d_0}{\left(1 + \frac{\rho}{\Delta \rho}\right)} \frac{\frac{\delta F}{F_0}}{\left(1 + \frac{\delta F}{F_0}\right)}. \quad (8)$$

214 When $|\delta F| \sim F_0$ we should expect the amplitude of topography h in degree-2 to reach
 215 about $d_0/20$. If $h \leq 0.3$ km, then this is only true when $d_0 \leq 6$ km—which is thinner
 216 than the ~ 23 km minimum average thickness we expect for Io’s lithosphere (Section
 217 S1 of Supplement 1).

218 **3.2 Pratt Isostasy**

219 Under Pratt isostasy, we expect topography to be the result of density variations
 220 in the lithosphere. Traditionally, Pratt isostasy also assumes the base of the lithosphere
 221 is “flat” and there is no basal topography. For Io, this is less certain (cf., Spencer et al.,
 222 2021), but as a combination of Pratt and Airy would be dominated by the effects of Airy
 223 isostasy, we assume this traditionally flat basal topography as an endmember case. To
 224 maintain constant pressure at depth, density variations in the lithosphere $\delta \rho$ from a reference
 225 average lithospheric density ρ_0 are

$$\delta \rho = -\rho_0 \frac{h}{d_0}. \quad (9)$$

226 Assuming density variations are due only to thermal expansion or contraction of
 227 the lithosphere, we relate the change in crustal density to the change in the lithosphere’s

228 average temperature $\delta\bar{T}$ from some reference temperature \bar{T}_0 for a thermal expansivity
 229 α :

$$\delta\bar{T} = -\frac{\delta\rho}{\alpha\rho_0} = \frac{\delta d}{\alpha d_0} = \frac{h}{\alpha d_0}, \quad (10)$$

230 where the final equality makes use of the fact that $\delta d = h$ in Pratt isostasy. It then behooves
 231 us to calculate the average temperature of the lithosphere and relate it to the heat flux
 232 through the lithosphere. O'Reilly and Davies (1981) provide the temperature profile as
 233 a function of depth z (where $z = 0$ is the surface, and $z = d$ is the base of the lithosphere):

$$T(z) = T_s + (T_m - T_s) \frac{e^{vz/\kappa} - 1}{e^{vd/\kappa} - 1}. \quad (11)$$

234 By taking the integral of Equation 11, we can find the average temperature of the lithosphere:

$$\bar{T} = \frac{1}{d} \int_0^d T(z) dz, \quad (12)$$

235 Finding

$$\bar{T} = T_s + (T_m - T_s) \left(\frac{\kappa}{vd} - \frac{1}{e^{vd/\kappa} - 1} \right), \quad (13)$$

236 which agrees that for high emplacement rates or thick lithospheres, most heat transport
 237 is accomplished by the advection of magma and thus the lithosphere's average temperature
 238 will be closer to the the surface temperature than the melting temperature. If v or d approaches
 239 0, we can take the approximation $e^{vd/\kappa} \approx 1 + \frac{vd}{\kappa} + \frac{1}{2} \left(\frac{vd}{\kappa} \right)^2$ and we find that \bar{T} approaches
 240 $(T_m - T_s)/2$, which is what we expect in the case without heat pipes. Spencer et al. (2021)
 241 also assume Pratt isostasy in Io's lithosphere would be dominated by thermal expansion.

242 In our study, we explicitly vary the volcanic emplacement rate v and lithospheric
 243 thickness d , but hold the surface temperature T_s constant. T_m can vary in some unknown
 244 manner, so in our formalism for translating the topography δd into heat flux F via Pratt
 245 isostasy, we want to eliminate the dependence of T_m before we continue our derivation.
 246 We can rearrange Equation 13 to find

$$T_m - T_s = \frac{\bar{T} - T_s}{\frac{\kappa}{vd} - \frac{1}{e^{vd/\kappa} - 1}}. \quad (14)$$

247 Substituting Equation 14 into Equation 1 and rearranging, we find

$$F = v\rho \left[\Delta H_f + \frac{vd}{\kappa} (\bar{T} - T_s) \frac{e^{vd/\kappa}}{e^{vd/\kappa} - 1 - \frac{vd}{\kappa}} \right]. \quad (15)$$

248 For our minimum values of v , d , and F (Table 1), vd/κ is at minimum 7.8; implying
 249 $e^{vd/\kappa} > 2400$. Then, the fraction $e^{vd/\kappa} / (e^{vd/\kappa} - 1 - \frac{vd}{\kappa})$ is only greater than unity by

250 a maximum of 0.4%, meaning we may safely neglect the fraction for our consideration
 251 of Pratt isostasy. Simpler now, we find,

$$F \approx v\rho \left[\Delta H_f + \frac{vd}{\kappa} C_p (\bar{T} - T_s) \right]. \quad (16)$$

252 **3.2.1 Constant v case**

253 If we assume emplacement rate v is uniform across Io's surface in the case of Pratt
 254 isostasy, we can substitute $v = v_0$ into Equation 16. Then, one would expect the difference
 255 in heat flux from average δF to be

$$\delta F \approx \frac{v_0^2 \rho C_p}{\kappa} [d_0 \delta \bar{T} + h(\bar{T}_0 - T_s) + h \delta \bar{T}]. \quad (17)$$

256 When we substitute $\delta \bar{T} = h/(\alpha d_0)$ (Equation 10) into Equation 17, we find the
 257 variation in heat flux through Io's lithosphere under Pratt isostasy and constant volcanic
 258 emplacement $v = v_0$ as,

$$\delta F \approx \frac{v_0^2 h \rho C_p}{\kappa} \left[\frac{1}{\alpha} \left(1 + \frac{h}{d_0} \right) + (\bar{T}_0 - T_s) \right]. \quad (18)$$

259 In the first term within the square brackets, we expect $\frac{h}{d_0} \ll 1$, meaning we can drop
 260 the second term within those parentheses for this approximation. A reasonable volumetric
 261 thermal expansivity for rock at \bar{T} is $\alpha \sim 3 \times 10^{-5} \text{ K}^{-1}$, meaning that $\bar{T}_0 - T_s \ll \alpha^{-1}$,
 262 and we may drop that second term. Thus, our relationship between topography h and
 263 variation in tidal heating δF can be reduced to,

$$\delta F \simeq \frac{v_0^2 \rho C_p}{\kappa \alpha} h. \quad (19)$$

264 Keeping in mind that $F_0 \sim F_{adv}$, we can account for variations in F as a factor
 265 of itself by dividing both sides of Equation 19 by F_0 or F_{adv} ,

$$\frac{\delta F}{F_0} \sim h \frac{v_0}{\kappa} \frac{C_p \frac{1}{\alpha}}{\Delta H_f + C_p (T_m - T_s)}. \quad (20)$$

266 Solving now for the topography h ,

$$h \sim \frac{\delta F}{F_0} \frac{\kappa}{v_0} \alpha \left[\frac{\Delta H_f}{C_p} + (T_m - T_s) \right]. \quad (21)$$

267 If heat flux varies on the order of itself ($|\delta F| \sim F_0$), then we expect the amplitude of
 268 h to reach about $h \sim 172 \text{ m} \times \frac{\delta F}{F_0} \frac{10.7 \text{ mm yr}^{-1}}{v_0}$ (where $v_0 = 10.7 \text{ mm yr}^{-1}$ is the minimum
 269 average volcanic emplacement expected for the minimum observed average heat flux of

270 $F \sim 2 \text{ W m}^{-2}$), which would create long-wavelength topography *less* than the maximum
 271 possible degree-2 topography (as limited by our uncertainty, Section S2 of Supplement
 272 1).

273 3.2.2 $v \propto F$ case

274 When v is instead proportional to F in the case of Pratt isostasy, we substitute $v =$
 275 $v_0 F/F_0$ into Equation 16 and rearrange to find

$$\frac{F}{F_0} \approx \frac{F_0 - v_0 \rho \Delta H_f}{\frac{v_0 d}{\kappa} v_0 \rho C_p (\bar{T} - T_s)}. \quad (22)$$

276 In this case, the variation in F is due to variation in the $1/[d(\bar{T}-T_s)]$ term. Neither
 277 d nor \bar{T} are expected to vary greatly, and thus we make the approximation

$$\delta \left[\frac{1}{d(\bar{T} - T_s)} \right] \simeq - \frac{[d_0 \delta \bar{T} + h(\bar{T}_0 - T_s)]}{d_0^2 (\bar{T}_0 - T_s)^2}. \quad (23)$$

278 Thus,

$$\frac{\delta F}{F_0} \simeq - \frac{(F_0 - v_0 \rho \Delta H_f) [d_0 \delta \bar{T} + \delta d (\bar{T}_0 - T_s)]}{v_0^2 d_0^2 k (\bar{T}_0 - T_s)^2}. \quad (24)$$

279 When we substitute $\delta \bar{T} = h/(\alpha d_0)$ (Equation 10) into Equation 24, we find the
 280 variation in heat flux through Io's lithosphere under Pratt isostasy and volcanic emplacement
 281 rate proportional to heat flux variations $v = v_0 F/F_0$ as,

$$\frac{\delta F}{F_0} \simeq - \frac{(F_0 - v_0 \rho \Delta H_f) \left[\frac{1}{\alpha} + (\bar{T}_0 - T_s) \right] h}{v_0^2 d_0^2 k (\bar{T}_0 - T_s)^2}. \quad (25)$$

282 Then, using Equation 14, the $\bar{T}_0 - T_s$ term within the square brackets can be substituted
 283 with $\bar{T}_0 - T_s = (T_{m,0} - T_s) \left[\frac{\kappa}{v d} - \frac{1}{\exp(v d / \kappa) - 1} \right]$. Assuming $T_m - T_s = 1,500 \text{ K}$, this
 284 term is a *maximum* of 193 K (for our minimum v_0 and d). Meanwhile, α^{-1} is *always* much
 285 greater than $(\bar{T}_0 - T_s)$. Thus, our relationship between topography and variation in tidal
 286 heating δF can be reduced to,

$$\frac{\delta F}{F} \sim \frac{F_0 - v_0 \rho \Delta H_f}{\frac{v_0 d_0}{\kappa} v_0 \rho C_p (\bar{T}_0 - T_s)} \times \frac{-1}{\alpha (\bar{T}_0 - T_s)} \frac{h}{d_0}. \quad (26)$$

287 If one substitutes $\bar{T}_0 - T_s$ with Equation 10, they will find the denominator of the first
 288 fraction in Equation 26 will very nearly be equivalent to $F_0 - v_0 \rho \Delta H_f$ (Equation 1) and
 289 thus reduce the fraction to 1. Then,

$$\frac{\delta F}{F_0} \sim - \frac{v_0}{\kappa} \frac{h}{\alpha (T_{m,0} - T_s)}. \quad (27)$$

290 Finally, rearranging to solve for h ,

$$h \sim \frac{\delta F}{F_0} \frac{\kappa}{v_0} \alpha (T_m - T_s). \quad (28)$$

291 If heat flux varies on the order of itself ($|\delta F| \sim F_0$), then we expect the amplitude of
 292 h to reach about $h \sim 132 \text{ m} \times \frac{\delta F}{F_0} \frac{10.7 \text{ mm yr}^{-1}}{v_0}$.

293 4 Implications and Discussion

294 Should Io have a magma ocean, we might expect its lithosphere to experience Airy
 295 isostasy rather than Pratt isostasy. However, when assuming Airy isostasy, we find in both
 296 the constant $v = v_0$ and proportional $v \propto F$ cases of volcanic emplacement that the
 297 resulting degree-2 topography is far greater than the maximum possible topography as
 298 limited by our uncertainty (Figure 1). Thus, it is impossible for Io lithosphere's lithosphere
 299 to be in Airy isostasy if the variation in heat flux is as great as one would expect from
 300 tidal heating. Instead, this would imply that the heat flux is a mostly uniform background.
 301 Io cannot generate this much heat radioactively, so if Io were in Airy isostasy, some additional
 302 process would need either to erase either Io's topography in response to strong tidal heat
 303 variations *or* any spatial variation in the tidal heat that would produce this topography.

304 However, it *is* possible for Io to produce its expected long-wavelength topography
 305 while under strong tidal heating variations on the order of its average tidal heat flux—*if*
 306 Io's lithosphere operates under Pratt isostasy. This is true both when volcanic emplacement
 307 rate is uniform across Io's surface and when variation in volcanic emplacement rate is
 308 proportional to variations in tidal heating (Figure 1). In both cases, we expect the amplitude
 309 of degree-2 topography to reach about $\sim 150 \text{ m}$ when average volcanic emplacement rate
 310 v is that which is expected for the observed minimum average heat flow (Table 1).

311 Before eliminating the possibility of Airy isostasy, we explore the reasons why there
 312 may not be significant topography in response to expected variations of tidal heating.

313 4.1 Topographic relaxation

314 One reason why Io might not have significant topography if it were in Airy isostasy
 315 could be lower crustal (here, lithospheric) flow. The warmest portion of the lithosphere
 316 will tend to have the lowest viscosity and will flow laterally in response to horizontal pressure
 317 gradients (e.g., McKenzie et al., 2000; Nimmo & Stevenson, 2001; Nimmo, 2004). That

318 is, the deepest roots of the lithosphere will naturally want to smooth out and reduce its
 319 basal topography. Typically, this timescale is much longer than that for attaining isostatic
 320 topography in the first place (e.g., Nimmo & Stevenson, 2001). We examine here if this
 321 holds true for Io as well.

322 As for the crusts of many planetary bodies, the dynamic viscosity η of Io's lithosphere
 323 is expected to vary exponentially with its temperature, $\eta \propto \exp[Q_A/(R_G T)]$, where
 324 Q_A is the activation energy of the rock that makes up the lithosphere and R_G is the universal
 325 gas constant. Because the viscosity depends exponentially upon the temperature within
 326 the lithosphere, we expect only the base of Io's lithosphere to have a viscosity low enough
 327 to flow laterally. The thickness of this flowing region is a few times some characteristic
 328 lengthscale δ_{flow} . Then, the timescale τ_{rel} to relax (reduce) the amplitude of sinusoidal
 329 variations in topography in spherical harmonic degree l by a factor of e is provided by
 330 Nimmo (2004) as

$$\tau_{rel} = \frac{\eta_0}{\Delta\rho g} \left(\frac{R_0}{l}\right)^2 \frac{1}{\delta_{flow}^3}, \quad (29)$$

331 where η_0 is the reference viscosity at the base of the lithosphere (where $T = T_m$), and
 332 R_0 is Io's average radius (listed in Table 1). We focus on spherical harmonic degree $l =$
 333 2 , where the greatest variation in tidal heating is expected. At $l = 2$, the wavelength
 334 of topographic variation is half of Io's circumference.

335 As one might expect from a lengthscale that characterizes the thickness of the flowing
 336 region of a lithosphere when its viscosity depends exponentially on temperature, δ_{flow}
 337 depends on the vertical temperature gradient $\frac{\partial T}{\partial z}$ at the base of the lithosphere, where
 338 z is depth measured from Io's surface. Following Nimmo and Stevenson (2001), if viscosity
 339 depends on temperature as $\eta \sim e^{Q_A/(R_G T)}$ and the temperature gradient at some distance
 340 $\Delta z = d - z$ above the base of the lithosphere (thickness d) is approximately linear, then

$$\exp\left(\frac{Q_A}{R_G T}\right) \approx \exp\left(\frac{Q_A}{R_G T_m}\right) \exp\left(\frac{\Delta z}{\delta_{flow}}\right). \quad (30)$$

341 Thus,

$$\delta_{flow} \simeq \frac{R_G}{Q_A} \frac{T_m^2}{\left.\frac{\partial T}{\partial z}\right|_{z=d}} \quad (31)$$

342 (cf., Nimmo & Stevenson, 2001; Nimmo, 2004).

343 Were Io's lithosphere to be in a purely conductive regime (very thin crust), we would
 344 find $\delta_{flow} = R_G k T_m^2 / (Q_A F_{cond})$. However, because we expect Io to have a lithospheric
 345 thickness $d > 23$ km (Section S1 of Supplement 1), we must instead take the derivative

346 of Equation 11 to find

$$\delta_{flow} = \frac{R_G \kappa}{Q_A v} \frac{T_m^2}{(T_m - T_s)}. \quad (32)$$

347 This is substantially smaller than what one expects in a purely conductive regime, by
 348 a factor of about $3F_{adv}/(4F_{cond})$. This is because the temperature profile we expect in
 349 Io's lithosphere (Equation 11) is relatively close to the surface temperature T_s until $z \rightarrow$
 350 d and the temperature exponentially climbs to T_m . Assuming Io's lithosphere has an activation
 351 energy of $\sim 300 \text{ kJ mol}^{-1}$, δ_{flow} is only about 100 m.

352 Such a low δ_{flow} vastly increases the amount of time it would take to relax Io's isostatic
 353 topography. Meanwhile, the timescale to attain topography in isostatic equilibrium τ_{iso}
 354 is $\tau_{iso} \sim \eta_M l / (2\pi \rho_M g R_0)$ (Nimmo & Stevenson, 2001), where η_M is mantle viscosity
 355 and ρ_M is mantle density. Then, a comparison of the two timescales yields

$$\frac{\tau_{rel}}{\tau_{iso}} = 2\pi \frac{\eta_0}{\eta_M} \frac{\rho_M}{\Delta\rho} \left(\frac{R_0}{\delta_{flow} l} \right)^3, \quad (33)$$

356 where with our preferred values (Table 1) is about $10^{14} \eta_0/\eta_M$. This means that for lower
 357 crustal flow to reasonably erase any long-wavelength topography due to variations in tidal
 358 heating, Io's mantle would need to be 10^{11} times more viscous than the base of its lithosphere.
 359 While the viscosity profile of Io is poorly constrained (cf., Lainey et al., 2009; Bierson
 360 & Nimmo, 2016; Steinke et al., 2020a, 2020b; Spencer et al., 2021), such a contrast sparks
 361 incredulity. Thus, it is unlikely that in the event of Airy isostasy, topography would be
 362 subdued by lower lithospheric flow.

363 4.2 Tidal heat redistribution

364 Another possibility to investigate is the redistribution of tidal heat flux into a more
 365 uniform heating pattern. Assuming the case where volcanic emplacement rate $v \propto F$,
 366 we may rearrange Equation 8 to find

$$\frac{|\delta F|}{F_0} = \frac{1}{1 + \frac{d_0}{h(1 + \frac{\rho}{\Delta\rho})}}. \quad (34)$$

367 For maximum degree-2 topography of $h \sim 0.3 \text{ km}$ (Section S2 of Supplement 1)
 368 and minimum lithosphere thickness of $d_0 \sim 23 \text{ km}$ (Section S1 of Supplement 1), we
 369 find that variations in heat flux must have a maximum $|\frac{\delta F}{F_0}| < 0.17$ to not violate the
 370 observed topography (see also Figure 1). By examining the volcano distribution, Steinke
 371 et al. (2020b) find that the magnitude of degree-2 coefficients of volcano density vary from

372 0.02 to $0.146\times$ the average volcano density, which is consistent with our finding that degree-2
 373 variations in heat flux are below 0.17 of the average. Hamilton et al. (2013) likewise argue
 374 that if Io's volcano distribution is related to a tidal heat distribution, then that heating
 375 pattern is approximately 20% tidal heating in Io's aesthenosphere with the rest either
 376 a uniform heat distribution or deep mantle heating. As less than 1% of Io's total heat
 377 production is radiogenic, then a uniform heat distribution would need to have been a tidal
 378 heating pattern that was blurred into appearing uniform.

379 The observed variation in surface heat flux δF_O may be related to the originally
 380 produced heat flux δF_P by some blurring function $B(l)$ that depends on the spherical
 381 harmonic degree l (e.g., Steinke et al., 2020a, 2020b). This assumes that there exists a
 382 convective layer beneath the lithosphere (typically the aesthenosphere) that produces
 383 its own heat tidally. Following Tackley (2001); Steinke et al. (2020a, 2020b), we find this
 384 blurring function to be

$$B(l) = \frac{R_0 \pi}{l d_{conv}} C_B \text{Ra}_H^{-\beta}, \quad (35)$$

385 where d_{conv} is the thickness of the convecting layer, C_B and β are constants related to
 386 the blurring of the heat flux variations, and Ra_H is the Rayleigh-Roberts number (sometimes
 387 referred to as the internal-heating Rayleigh number), which characterizes the convective
 388 transport of heat-producing material as compared to the diffusion of its heat and is defined
 389 as

$$\text{Ra}_H = \frac{\rho g \alpha H d_{conv}^5}{k \eta_{conv} \kappa}, \quad (36)$$

390 where H is the thermal productivity in the mantle in units of power per mass and η_{conv}
 391 is the dynamic viscosity of the convecting layer. Following Steinke et al. (2020a, 2020b),
 392 we approximate $H = f_{cc} F_P / d_{conv}$, where f_{cc} is the fraction of tidal heating produced
 393 in the convective layer F_P that is transported through the mantle by conduction and convection
 394 (as opposed to bouyant magmatism through the mantle).

395 In order for the spatial distribution of volcano density to resemble a tidal heating
 396 pattern whose heat flux varies approximately $\leq 17\%$ of the average heat flow, then $B(2) \leq$
 397 0.17. That is,

$$\text{Ra}_H \geq \left(\frac{R_0}{d_{conv}} \frac{\pi C_B}{2 \cdot 0.17} \right)^{1/\beta}. \quad (37)$$

398 When heating is uniform within the convective layer, $C_B = 4.413$ and $\beta = 0.2448$, while
 399 when the heating is focused at the boundary of the layer, $C_B = 2.869$ and $\beta = 0.2105$
 400 (Tackley, 2001). Depending on the regime then, this would mean Ra_H has to be greater

401 than about 10^{13} to 10^{14} (assuming a convective layer thickness of 50 km) to reduce degree-2
 402 tidal heating variations to 17%.

403 For constants in Table 1, we find this implies for such blurring to occur,

$$\frac{\eta_{conv}}{f_{cc}} \leq 7 \times 10^{10} \text{ Pa s} \left(\frac{F_P}{2 \text{ W m}^{-2}} \right) \left(\frac{d_{conv}}{50 \text{ km}} \right)^{4+\frac{1}{\beta}}. \quad (38)$$

404 Steinke et al. (2020b) find that f_{cc} is likely < 0.2 . This then requires that if there were
 405 a circulating layer, its viscosity would be $< 10^{10}$ Pa s, which is lower than most estimates
 406 of asthenospheric viscosity (cf., Tackley, 2001; Steinke et al., 2020b). To achieve such a
 407 low viscosity might require the convecting layer to be a magma ocean—but then the amount
 408 of tidal heating produced within the convecting layer F_P would be greatly diminished.
 409 Furthermore, any heat produced by a magma ocean tides (e.g. Tyler et al., 2015) would
 410 be mainly due to the friction of the magma ocean dragging against the overlying lithosphere
 411 (cf. for ocean tides within icy satellites, Chen et al., 2014; Hay & Matsuyama, 2019).

412 The extent to which a magma ocean may instead redistribute a tidal heating pattern
 413 generated from *beneath* it rather than within it is presently unclear. However, we may
 414 draw an analogy with Europa, where it has been found that when ocean circulation has
 415 a weak dependence on rotation, such circulation has minimal effect upon the dispersion
 416 of tidal heating distributions from beneath (Soderlund et al., 2023). Thermal circulation
 417 in a potential magma ocean within Io would have an even weaker dependence on rotation,
 418 owing to the much higher viscosity of magma compared to water (a deeper discussion
 419 on how to characterize heat transfer in the circulating oceans of icy satellites may be found
 420 in Soderlund, 2019). Thus, we find it unlikely that a tidal heating pattern is redistributed
 421 by a convecting layer—whether the tidal heat is produced within a convecting aesthenosphere
 422 or produced beneath a convecting magma ocean.

423 5 Conclusions

424 Ultimately, we find that the maximum amplitude of isostatic topography that results
 425 from spatial variations in tidal heating across Io is irreconcilable with the expected spatial
 426 variation in tidal heating if we assume that Io’s lithosphere operates under Airy isostasy.
 427 The amplitude of tidal heating variation in spherical harmonic degree 2 is expected to
 428 be on the order of average tidal heating. Instead, the assumption of Airy isostasy requires
 429 an amplitude of tidal heating variation $< 17\%$ of the average heat flow. A convective
 430 layer can produce and redistribute tidal heating into a relatively uniform heating pattern,

431 but requires that this convective layer both produces most of Io's tidal heat *and* that
432 this layer have an extremely low viscosity $< 10^{10}$ Pa s. An aesthenosphere could produce
433 adequate internal tidal heating (i.e., not from drag at the base of the lithosphere) while
434 a magma ocean may have a low enough viscosity, but neither possibility fulfills both conditions.

435 If we instead assume that Io's lithosphere operates under Pratt isostasy, then the
436 predicted isostatic topography is consistent with the maximum allowed by the observations.
437 Because we rule out Airy isostasy in favor of Pratt isostasy, this implies that a magma
438 ocean is unlikely. This can soon be tested, as Juno's upcoming orbits of Jupiter will bring
439 it close to Io. Already, recent infrared imagery has been used to analyze the distribution
440 of Io's volcanic heat flow. Pettine et al. (2023) find that the tidal heating pattern implied
441 by Io's volcano distribution is anti-correlated with a global magma ocean and instead
442 suggests tidal heating in the aesthenosphere (cf., Davies et al., 2023), demonstrating a
443 similar conclusion to our own using an entirely different dataset and method. Upcoming
444 Juno flybys also allow the measurement of new gravitational data (Keane et al., 2022)
445 that supplements measurements from older spacecraft. Such gravity observations could
446 unveil Io's Love number k_2 , which characterizes Io's tidal response. A high value of $k_2 \sim$
447 0.5 is expected if Io has a magma ocean, while a lower value $k_2 \sim 0.1$ is expected without
448 a magma ocean (Bierson & Nimmo, 2016; de Kleer et al., 2019). Thus, we predict that
449 if k_2 is measured for Io with Juno data, it will be low.

450 **Open Research Section**

451 This paper is purely theoretical, only deriving equations to apply to previously observed
452 physical parameters. As such, no datasets were analyzed or produced for this paper. The
453 python code used to create Figure 1 has been uploaded to the Dryad Repository and is
454 listed in our References as Gyalay and Nimmo (2023b).

455 **Acknowledgments**

456 FN received funding from NASA Grant 80NSSC21K1802.

457 **References**

- 458 Beuthe, M. (2013). Spatial patterns of tidal heating. *Icarus*, *223*(1), 308–329. doi:
459 10.1016/j.icarus.2012.11.020
460 Beuthe, M. (2021). Isostasy with Love – i: elastic equilibrium. *Geophysical Journal*

- 461 *International*, 225(3), 2157–2193. doi: 10.1093/gji/ggab073
- 462 Bierson, C. J., & Nimmo, F. (2016). A test for Io’s magma ocean: modeling tidal
463 dissipation with a partially molten mantle. *Journal of Geophysical Research:*
464 *Planets*, 121(11), 2211–2224. doi: 10.1002/2016JE005005
- 465 Carr, M. H., Masursky, H., Strom, R. G., & Terrile, R. J. (1979). Volcanic features
466 of Io. *Nature*, 280(5725), 729–733. doi: 10.1038/280729a0
- 467 Carr, M. H., McEwen, A. S., Howard, K. A., Chuang, F. C., Thomas, P., Schuster,
468 P., . . . Galileo Imaging Team (1998). Mountains and calderas on Io: Possible
469 implications for lithosphere structure and magma generation. *Icarus*, 135(1),
470 146–165. doi: 10.1006/icar.1998.5979
- 471 Chen, E. M. A., Nimmo, F., & Glatzmaier, G. A. (2014). Tidal heating in icy
472 satellite oceans. *Icarus*, 229, 11–30. doi: 10.1016/j.icarus.2013.10.024
- 473 Davies, A. G., Perry, J., Williams, D. A., & Nelson, D. M. (2023). *Io’s polar volcanic*
474 *thermal emission indicative of magma ocean and shallow tidal heating models.*
475 (Preprint on Arxiv, <https://doi.org/10.48550/arXiv.2310.12382>) doi:
476 10.48550/arXiv.2310.12382
- 477 de Kleer, K., McEwen, A. S., Park, R. S., Bierson, C. J., Davies, A. G.,
478 DellaGiustina, D. N., . . . Schneider, N. M. (2019). *Tidal heating: Lessons*
479 *from Io and the Jovian system.* Final Report for the Keck Institute for Space
480 Studies.
- 481 Gyalay, S., & Nimmo, F. (2023a). Estimates for Tethys’ moment of inertia,
482 heat flux distribution, and interior structure from its long-wavelength
483 topography. *Journal of Geophysical Research: Planets*, 128(2). doi:
484 10.1029/2022JE007550
- 485 Gyalay, S., & Nimmo, F. (2023b). *Isostatic response of io’s topography*
486 *to the spatial variation of its tidal heating.* Dataset. Dryad.
487 Retrieved from [https://datadryad.org/stash/share/Y0zgrXbQG](https://datadryad.org/stash/share/Y0zgrXbQG_GixJeSwZfZU98JdovcqV1yJYAZGPZLhw)
488 [_GixJeSwZfZU98JdovcqV1yJYAZGPZLhw](https://datadryad.org/stash/share/Y0zgrXbQG_GixJeSwZfZU98JdovcqV1yJYAZGPZLhw) (This is a private URL for peer
489 review. The repository will be made public with a doi for the final draft.)
- 490 Hamilton, C. W., Beggan, C. D., Still, S., Beuthe, M., Lopes, R. M. C., Williams,
491 D. A., . . . Wright, W. (2013). Spatial distribution of volcanoes on Io:
492 Implications for tidal heating and magma ascent. *Earth and Planetary Science*
493 *Letters*, 361, 272–286. doi: 10.1016/j.epsl.2012.10.032

- 494 Hay, H., & Matsuyama, I. (2019). Nonlinear tidal dissipation in the subsurface
 495 oceans of Enceladus and other icy satellites. *Icarus*, *319*, 68–85. doi: 10.1016/
 496 j.icarus.2018.09.019
- 497 Hemingway, D., & Masuyama, I. (2017). Isostatic equilibrium in spherical
 498 coordinates and implications for crustal thickness on the Moon, Mars,
 499 Enceladus, and elsewhere. *Geophysical Research Letters*, *44*(15), 7695–7705.
 500 doi: 10.1002/2017GL073334
- 501 Jaeger, W. L., Turtle, E. P., Keszthelyi, L. P., Radebaugh, J., McEwen, A. S., &
 502 Pappalardo, R. T. (2003). Orogenic tectonism on Io. *Journal of Geophysical*
 503 *Research: Planets*, *108*(E8). doi: 10.1029/2002JE001946
- 504 Keane, J. T., de Kleer, K., & Spencer, J. (2022). Perspective: the future exploration
 505 of Io. *Elements*, *18*(6), 399–404. doi: 10.2138/gselements.18.6.399
- 506 Keszthelyi, L., & McEwen, A. (1997). Magmatic differentiation of Io. *Icarus*, *130*(2),
 507 437–448. doi: 10.1006/icar.1997.5837
- 508 Khurana, K. K., Jia, X., Kivelson, M. G., Nimmo, F., Schuber, G., & Russell, C. T.
 509 (2011). Evidence of a global magma ocean in Io’s interior. *Science*, *332*(6034),
 510 1186–1189. doi: 10.1126/science.1201425
- 511 Lainey, V., Arlot, J., Karatekin, O., & Van Hoolst, T. (2009). Strong tidal
 512 dissipation in Io and Jupiter from astrometric observations. *Nature*, *459*,
 513 957–959. doi: 10.1038/nature08108
- 514 Matusyama, I. N., Steinke, T., & Nimmo, F. (2022). Tidal heating in Io. *Elements*,
 515 *18*(6), 374–378. doi: 10.2138/gselements.18.6.374
- 516 McEwen, A. S., Keszthelyi, L. P., Lopes, R., Schenk, P. M., & Spencer, J. R.
 517 (2004). Jupiter: The planet, satellites and magnetosphere. In F. Bagenal,
 518 T. E. Dowling, & W. B. McKinnon (Eds.), (pp. 307–328). Cambridge
 519 University Press.
- 520 McKenzie, D., Nimmo, F., Jackson, J. A., Gans, P. B., & Miller, E. L. (2000).
 521 Characteristics and consequences of flow in the lower crust. *Journal of*
 522 *Geophysical Research: Solid Earth*, *105*, 11029–11046. doi: 10.1029/
 523 1999JB900446
- 524 Miyazaki, Y., & Stevenson, D. J. (2022). a subsurface magma ocean on Io: exploring
 525 the steady state of partially molten planetary bodies. *Planetary Science*
 526 *Journal*, *3*(11), 256. doi: 10.3847/PSJ/ac9cd1

- 527 Nash, D., Yoder, C., Carr, M., Gradie, J., & Hunten, D. (1986). Satellites. In
 528 J. A. Burns & M. S. Matthews (Eds.), (chap. Io: history of studies and current
 529 level of understanding of this satellite). University of Arizona Press.
- 530 Nimmo, F. (2004). Non-Newtonian topographic relaxation on Europa. *Icarus*,
 531 *168*(1), 205–208. doi: 10.1016/j.icarus.2003.11.022
- 532 Nimmo, F., & Stevenson, D. J. (2001). Estimates of Martian crustal thickness from
 533 viscous relaxation of topography. *Journal of Geophysical Research: Planets*,
 534 *106*(E3), 5085–5098. doi: 10.1029/2000JE001331
- 535 O’Reilly, T. C., & Davies, G. F. (1981). Magma transport of heat on Io: A
 536 mechanism allowing a thick lithosphere. *Geophysical Research Letters*, *8*(4),
 537 313–316. doi: 10.1029/GL008i004p00313
- 538 Peale, S. J., Cassen, P., & Reynolds, R. T. (1979). Melting of Io by tidal dissipation.
 539 *Science*, *203*(4383), 892–894. doi: 10.1126/science.203.4383.892
- 540 Pettine, M., Imbeah, S., Rathbun, J., Hayes, A., Lopes-Gautier, R., Mura, A., ...
 541 Bertolino, S. (2023). *JIRAM observations of volcanic flux on Io: Distribution*
 542 *and comparison to tidal heat flow models.* (Preprint on Arxiv, [https://](https://doi.org/10.48550/arXiv.2308.05717)
 543 doi.org/10.48550/arXiv.2308.05717) doi: 10.48550/arXiv.2308.05717
- 544 Rathbun, J. A., Spencer, J. R., Lopes, R. M., & Howell, R. R. (2014). Io’s active
 545 volcanoes during the New Horizons era: insights from New Horizons imaging.
 546 *Icarus*, *231*, 261–272. doi: 10.1016/j.icarus.2013.12.002
- 547 Rathbun, J. A., Spencer, J. R., Tamppari, L. K., Martin, T. Z., Barnard, L., &
 548 Travis, L. D. (2004). Mapping of Io’s thermal radiation by the Galileo
 549 photopolarimeter-radiometer (PPR) instrument. *Icarus*, *169*(1), 127–139.
 550 doi: 10.1016/j.icarus.2003.12.021
- 551 Schenk, P., Hargitai, H., Wilson, R., McEwen, A., & Thomas, P. (2001). The
 552 mountains of Io: Global and geological perspectives from Voyager and Galileo.
 553 *Journal of Geophysical Research: Planets*, *106*(E12), 33201–33222. doi:
 554 10.1029/2000JE001408
- 555 Schubert, G., Anderson, J. D., Spohn, T., & McKinnon, W. B. (2004). Jupiter:
 556 the planet, satellites, and magnetosphere. In F. Bagenal, T. E. Dowling, &
 557 W. B. McKinnon (Eds.), (Vol. 2, p. 281). Cambridge University Press.
- 558 Segatz, M., Spohn, T., Ross, M. N., & Schubert, G. (1988). Tidal dissipation,
 559 surface heat flow, and figure of viscoelastic models of io. *Icarus*, *75*(2),

- 560 187–206. doi: 10.1016/0019-1035(88)90001-2
- 561 Simonelli, D. P., Dodd, C., & Veverka, J. (2001). Regolith variations on Io:
562 Implications for bolometric albedos. *Journal of Geophysical Research: Planets*,
563 *106*(E12), 33241–33252. doi: 10.1029/2000JE001350
- 564 Soderlund, K. (2019). Ocean dynamics of outer solar system satellites. *Geophysical*
565 *Research Letters*, *46*(15), 8583–9299. doi: 10.1029/2018GL081880
- 566 Soderlund, K., Lemasquerier, D., & Bierson, C. (2023). Europa’s ocean translates
567 interior tidal heating patterns to the ice-ocean boundary. In *53rd Lunar and*
568 *Planetary Science Conference*.
- 569 Spencer, D. C., Katz, R. F., & Hewitt, I. J. (2021). Tidal controls on the
570 lithospheric thickness and topography of Io from magmatic segregation and
571 volcanism modelling. *Icarus*(in press). doi: 10.1016/j.icarus.2021.114352
- 572 Steinke, T., Hu, H., Höning, D., van der Wal, W., & Vermeersen, B. (2020a).
573 Tidally induced lateral variations of Io’s interior. , *335*. doi: 10.1016/
574 j.icarus.2019.05.001
- 575 Steinke, T., van Sliedregt, D., Vilella, K., van der Wal, W., & Vermeersen, B.
576 (2020b). Can a combination of convective and magmatic heat transport in
577 the mantle explain Io’s volcanic pattern? *Journal of Geophysical Research:*
578 *Planets*, *125*(12). doi: 10.1029/2020JE006521
- 579 Tackley, P. J. (2001). Convection in Io’s asthenosphere: redistribution of nonuniform
580 tidal heating by mean flows. *Journal of Geophysical Research: Planets*,
581 *106*(E12), 32971–32981. doi: 10.1029/2000JE001411
- 582 Tackley, P. J., Schubert, G., Glatzmaier, G. A., Schenk, P., Ratcliff, J. T., & Matas,
583 J.-P. (2001). Three-dimensional simulations of mantle convection in Io. *Icarus*,
584 *149*(1), 79-93. doi: 10.1006/icar.2000.6536
- 585 Turcotte, D., & Schubert, G. (2014). *Geodynamics* (3rd ed.). Cambridge University
586 Press, Cambridge (UK).
- 587 Tyler, R. H., Henning, W. G., & Hamilton, C. W. (2015). Tidal heating in a magma
588 ocean within Jupiter’s moon Io. *The Astrophysical Journal*, *218*(2), 22. doi: 10
589 .1088/0067-0049/218/2/22
- 590 Veeder, G. J., Matson, D. L., Johnson, T. V., Blaney, D. L., & Goguen, J. D.
591 (1994). Io’s heat flow from infrared radiometry: 1983-1993. *Journal of*
592 *Geophysical Research: Planets*, *99*, 17095–17162. doi: 10.1029/94JE00637